Journal of Nuclear Materials 409 (2011) 1–8

Contents lists available at ScienceDirect

Journal of Nuclear Materials

journal homepage: www.elsevier.com/locate/jnucmat

Thermodynamic study of the Np–Zr system

Saurabh Bajaj [a], Andres Garay [b], Alexander Landa [c], Per Söderlind [c], Patrice Turchi [c], Raymundo Arróyave [a,d,*]

[a] Department of Mechanical Engineering, Texas A&M University, College Station, TX 77843-3123, United States
[b] Centro de Investigación y de Estudios Avanzados del IPN (CINVESTAV), Unidad Querétaro, Querétaro, C.P. 76230, Mexico
[c] Lawrence Livermore National Laboratory, Livermore, CA 94551-0808, United States
[d] Materials Science and Engineering Program, Texas A&M University, College Station, TX 77843-3123, United States

ARTICLE INFO

Article history:
Received 25 May 2010
Accepted 7 October 2010
Available online 2 December 2010

ABSTRACT

A thermodynamic model of the Np–Zr system is developed using the CALPHAD method, and a review of previous work performed on this system is presented here. In general, results obtained are in good agreement with those proposed from experimental observations. It is found that the nature of reactivity of Np with Zr, is different from that of U and Pu: an expected elevation of melting point of Np–Zr alloys was not seen and a miscibility gap existed between the high-temperature bcc phases of Np and Zr. Formation enthalpy of the bcc phase obtained from the model is compared with results from KKR–ASA–CPA calculations. Lattice stabilities of various phases in the system are compared to values obtained from first-principles LDA and GGA calculations. The δ-$NpZr_2$ phase is modeled as a non-stoichiometric phase with a C32 structure, similar to what has been determined for the δ-phase in the U–Zr system. This phase is analogous to ω-phase in pure Zr, which is stabilized at high pressures. Two different possibilities for stability of the δ and ω phases have been proposed in the present work. Finally, calculated changes in enthalpy versus temperature are plotted for two alloys to guide future experimental work in resolving important issues in this system.

1. Introduction

Nuclear fission currently provides about 15% of the total global electric power and the fact that it produces greenhouse gas free energy [1], might play an important role in its contribution to the renewable energy sector. A major problem faced today with nuclear energy is waste disposal, with over 12,000 tons of radioactive nuclear waste being produced worldwide, every year [1]. The potential solution to this problem lies in the use of metallic nuclear fuels, particularly U–Pu–Zr alloys, that transmutate to long lived and high heat producing minor actinides such as Np, Am and Cm in fast breeder reactors, thus closing the nuclear fuel cycle [2] and achieve high 'burn-up' rates. The melting points of Np, Pu and U are relatively low for nuclear fuel applications (T_{fus}[Np] = 639 °C, T_{fus}[Pu] = 640 °C, T_{fus}[U] = 1135 °C [3,4]) which could pose a limitation to their use. Thus, Zr is alloyed with them to elevate the liquidus and also suppress inter-diffusion between the nuclear fuel and stainless steel cladding [5]. In this work we study one such alloy, Np–Zr, which may aid in predicting the nature of interactions in similar complex alloy systems.

Prior information available on the Np–Zr system is limited and contradictory. It was expected [6–9] that this system would be similar to the U–Zr and Pu–Zr systems, which are characterized by complete mutual solubility of the high-temperature (HT) body centered cubic (bcc) phases and an elevation in the melting points of Np alloys, relative to pure Np. However, according to Refs. [6–10], after performing several differential thermal analysis (DTA) and X-ray diffraction (XRD) experiments, it was confirmed that the HT bcc phases, γ-Np and β-Zr, were immiscible. It was also found that due to the low solubility of Zr in Np, there were only small changes in the melting points and transition temperatures of Np–Zr alloys. On the contrary, Rodríguez et al. [11] proposed a tentative phase diagram based on dilatometry, electron probe micro analysis (EPMA) and micrographic studies, that showed the Np–Zr system to be completely ideal. These experimental works are discussed in detail in Section 2.1.

Another debatable feature of the Np–Zr phase diagram is the structure and stability of the δ-$NpZr_2$ phase, analogous to the δ-UZr_2 phase in the U–Zr system [5,12,13] which is known to stabilize due to an increase in the d-band occupation of Zr [5,14]. Detailed discussions on this phase are offered in Sections 2.2, 2.4 and 5.4.

To improve our understanding of this system, it is necessary to study the equilibrium or partial/local equilibrium, along with kinetics of phase transformations and chemical reactions. Thus,

* Corresponding author. Address: 119 ENPH, Mail Stop 3123, Texas A&M University, College Station, TX 77843-3123, United States. Tel.: +1 979 845 5416; fax: +1 979 845 3081.
E-mail address: rarroyave@tamu.edu (R. Arróyave).

0022-3115/$ - see front matter © 2010 Elsevier B.V. All rights reserved.
doi:10.1016/j.jnucmat.2010.10.085

in this work, we develop a thermodynamic model based on the CALPHAD approach [15]. In this approach, Gibbs energies of all the phases taking part in equilibrium, are modeled through reliable and most recent experimental data. This thermodynamic modelling approach has many advantages: it provides an easy way to study how various equilibria and reactions are affected by various external factors and, it can be extrapolated to regions of temperatures and compositions which are not easily accessible by experiments. The use of such techniques becomes even more important as performing experiments still remains challenging for this class of systems.

2. Experimental data

In this section, we review details and results of various experiments performed on the Np–Zr system.

2.1. Phase diagram data

Gibson et al. [6] performed HT–DTA, up to 1500 °C, on Np–Zr alloys with 22, 48, 50, and 75 at.% Zr. For alloys with compositions 22, 48, and 50 at.% Zr, the sharp rise in liquidus temperatures was not observed from the DTA thermograms which suggests that the bcc phases of Np and Zr are immiscible. The low temperature peak due to the α-Np $\rightarrow$ β-Np transition was absent in the 48, 50, and 75 at.% Zr samples indicating the presence of a Zr-rich phase. By integration over peak areas of the heating and cooling curves, a high enthalpy was measured for the HT transition in these samples, which may be caused due to a Zr-rich intermediate phase, and we speculate it to be the δ-phase.

Gibson et al. [7] performed more extensive DTA studies on samples of compositions 22, 27, 48, 50, and 75 at.% Zr. Thermal events were recorded between 100 °C and 1400 °C, although no reproducible features were detected above 640 °C. Thermograms obtained for 22 and 27 at.% Zr alloys were similar to those obtained for pure Np, suggesting immiscibility and limited solute effect on the liquidus onset temperatures. It was also suggested from room temperature XRD [10] that due to larger cell volumes of α-Zr which was equilibrated with Np, than for just pure α-Zr, Np may have up to 10 at.% solubility in α-Zr. But, on the other hand, Zr has negligible solubility in α-Np.

Another group of experimentalists, Rodríguez et al. [11], performed dilatometry on three alloys of compositions 40, 72, and 91 at.% Zr. EPMA and microscopic examination of these samples showed complete mutual solubility between the γ-Np and β-Zr phases up to their respective melting points. This is in direct conflict with conclusions of the experimental works described before.

Okamoto et al. [9] performed XRD analysis on two samples, 67 and 75 at.% Zr, between 25 °C and 700 °C, and obtained results consistent with previous DTA [6,7], XRD [10] experiments and the phase diagram proposed by Gibson et al. [8], thus further strengthening the case of immiscibility.

2.2. δ-phase

It was determined [12,13] that the crystal structure of the δ-phase is a modified C32 (AlB_2 type) structure, with Zr atoms occupying the (0,0,0) position and a random mixture of U and Zr atoms occupying the $(\frac{2}{3},\frac{1}{3},\frac{1}{2})$ and $(\frac{1}{3},\frac{2}{3},\frac{1}{2})$ positions. XRD studies on the δ-phase pointed to a bcc structure instead of a structure with hexagonal symmetry and couple of reasons have been cited for this: transformation between the γ solid solution and δ-phase, a twinned crystal with four hexagonal cells [12]; and, the C32 structure is derived when two of three neighboring (1 1 1) planes in a bcc structure move towards one another along the [1 1 1] direction and collapse into one, hence compatible with the definition of the so called ω-phase as experimentally observed in Zr [14].

Okamoto et al. [9] found a greater intensity of δ-$NpZr_2$ phase in the 25 at.% Np alloy than in the 33 at.% Np alloy, predicting this phase to be non-stoichiometric. A decomposition temperature of 550 °C was assigned and it was concluded that this phase formed from γ-Np and α-Zr.

2.3. θ-phase

Diffraction lines observed by Gensini et al. [10] corresponded to a phase similar to the Pu_4Zr phase in the Pu–Zr system [16,17]. However, to the best of our knowledge, these is no experimental information available on the crystal structure, symmetry or stability of the θ-Np_4Zr phase and thus, it is modeled as a stoichiometric compound in our model.

2.4. The ω-phase of Zr

It is well known that zirconium metal undergoes hcp $\rightarrow$ ω and $\omega \rightarrow$ bcc transformations at pressures of 2.1–6.0 GPa [18] and $\sim$32 GPa [19], respectively. These phase transitions are accompanied by a change in the d-band occupation, which has also been observed when alloying zirconium with actinide elements [5,14,18]. The determination of the ground state phase of Zr, whether it is hcp or ω, has long been debated. According to experimental works in Refs. [19,20], at atmospheric pressure and temperatures below about 250 K, the ω-phase is found to be more stable than the hcp phase. In Ref. [20], formation enthalpy associated with the $\alpha \rightarrow \omega$ transition was found to be equal to -553 J/mol. Results from first-principles calculations performed in our study also indicate that the ω-phase is more stable than the hcp phase, although the difference in energy is only $\sim$1 kJ/mol. This is in agreement with results obtained in Refs. [21–24] which also show that this energy difference was small, with the ω-phase having a lower energy. Due to the uncertainty posed by this, both possible scenarios are taken into account in the present work. Models 1 and 2 will be calculated considering hcp and ω-phase, respectively, as the ground state of Zr and more details are given in Section 5.4.

3. Thermodynamic models

In this section, we describe the Gibbs energy functions of various phases in the model. G_m^{ϕ} denotes the molar Gibbs energy of phase ϕ, x_i is the molar fraction of component i and, ${}^{o}G_i^{\phi}$ defines the Gibbs energy of the phase containing the pure component i, obtained from the SGTE database [25].

3.1. Random solution

The liquid, orthorhombic and tetragonal phases are modeled as random solution phases, where the phase components may occupy spatial positions based purely on random substitution rather than on a preferential occupation of sites. The Gibbs energy of such a solution phase is given by:

$$G_m^{\phi} = \sum_{i=\mathrm{Np,Zr}} x_i {}^{o}G_i^{\phi} + RT \sum_{i=\mathrm{Np,Zr}} x_i log_e x_i + x_{\mathrm{Np}} x_{\mathrm{Zr}} L_{\mathrm{Np,Zr}}^{\phi} \quad (1)$$

where, $L_{\mathrm{Np,Zr}}^{\phi}$ is an interaction parameter used to incorporate the effects of non-ideal mixing. This parameter is further expanded using the Redlich–Kister formalism [26] as:

$$L_{\mathrm{Np,Zr}}^{\phi} = \sum_{v} L_{\mathrm{Np,Zr}}^{\phi} (x_{\mathrm{Np}} - x_{\mathrm{Zr}})^{v} \quad (2)$$

where, in case of regular solutions, $v = 0$ and in case of non-regular solutions, $v > 1$. This parameter is made temperature dependent:

$$^{v}L^{\phi}_{Np,Zr} = {}^{v}A + {}^{v}BT \quad (3)$$

where, ^{v}A and ^{v}B are model parameters to be optimized.

3.2. Sublattice model

The body centered cubic, hexagonal δ and θ phases are modeled as sublattice phases. This method is one of the most powerful and effective ways to model solution phases, such as interstitial and intermetallic compounds, in which a phase is composed of interlocking sublattices. The Gibbs energy expression for such a model is defined by:

$$G^{\phi}_{m} = \sum_{I0} P_{I0}(Y)\,{}^{o}G^{\phi}_{I0} + RT\sum_{s} N^{s}\sum_{i} {}^{s}y_i \log_e {}^{s}y_i + \sum_{Z>0}\sum_{IZ} P_{IZ}(Y)L^{\phi}_{IZ} \quad (4)$$

where P_{I0} is a product of the site fractions when each sublattice is occupied by only one component and P_{IZ} is the site fraction product when only one sublattice contains Z components and the remaining sublattices are occupied by one component. N^{s} is the total number of sites on sublattice s, and $^{s}y_i$ is called the site fraction and is given by:

$$^{s}y_i = \frac{n^{s}_{i}}{N^{s}} \quad (5)$$

where n^{s}_{i} is the number of atoms of component i on sublattice s.

In the case of regular solutions ($Z = 0$), mixing on each sublattice is independent of site occupations in the other sublattice. But, in the of sub-regular models ($Z > 0$), as shown in the Gibbs energy expression in Eq. (4) above, there is some dependence on site fractions of other sublattices which is added to the interaction parameter as follows:

$$L^{\phi}_{a,b:c} = {}^{1}y^{1}_{a}\,{}^{1}y^{1}_{b}\,y_c \sum_{v} {}^{v}L^{\phi}_{a,b:c}({}^{1}y_a - {}^{1}y_b)^{v} \quad (6)$$

This equation is valid for a two-sublattice system $(a,b)_1(c,d)_1$, wherein, there are four different combinations of mixing possibilities on the sublattices, one of which is shown above.

3.3. Evaluation of model parameters

The evaluation and optimization of the parameters, used in the description of the Gibbs energy functions, are carried out using the PARROT module of Thermo–Calc software [27] at atmospheric pressure (101.325 kPa). Given the contradictory nature of the data available on the phase diagram, variables for each phase were optimized, starting with low statistical weights and small number of iterations. The controversial body centered cubic phase, was optimized in an unbiased manner so that no preference was given to any of the previous experimental works that defined its character (miscible or immiscible). At the same time, care was taken to be within an acceptable range of solubilities and temperatures of the invariant reactions and phases, by increasing statistical weights appropriately. Another constraint used for this purpose was the driving force which is regarded as an affinity between reacting chemical species, and its magnitude defines the equilibrium of a phase at specified composition and temperature. The model was optimized until a balance had been achieved between the accuracies of the liquidus, solidus equilibrium lines and formation enthalpies of the bcc phase.

4. First-principles methodology

To validate the thermodynamic model developed, we performed first-principles calculations to evaluate formation enthalpies of the bcc phase and lattice stabilities in the Np–Zr alloy system. Lattice stabilities are relative Gibbs energies of pure elements in various crystal structures, which may consist of metastable or unstable structures, present in different regions of the phase diagram.

4.1. Evaluation of lattice stabilities

These calculations were performed within the Density Functional Theory (DFT) framework as implemented in the VASP code [28–31]. Ion-electron interactions were described using the Projector Augmented Wave (PAW) method [32,33]. The PAW potential was generated considering the 6d, 7s and 5f valence states for Np and 4s, 4p, 4d and 5s for Zr. Spin-polarized Local Density (LDA) [34] and Generalized Gradient Approximation (GGA–PBE) [35] were used to approximate the exchange-correlation functional. Convergence tests were first performed on the structures to limit total energy convergence to less than 0.005 eV. Plane wave energy cut-off of 600 eV was determined for the orthorhombic and tetragonal phases, whereas for the hcp phase, a value of 500 eV was deemed suitable. Integrations over the first Brillouin zone were made using k-point grid sets of $8 \times 10 \times 10$, $8 \times 8 \times 10$ and $12 \times 12 \times 10$ for the orthorhombic, tetragonal and hcp phases, respectively, generated according to the Γ-centered Monkhorst–Pack scheme [36].

4.2. Evaluation of formation enthalpies of the bcc phase

Formation enthalpies of bcc alloys of various compositions were computed using a scalar-relativistic Green's function technique based on the Korringa–Kohn–Rostoker (KKR) method within the atomic sphere approximation (ASA) [37–39], which is improved by addition of higher multipoles of the charge density [39], and the so called muffin-tin correction [40] to the electrostatic energy. The Generalized Gradient Approximation (GGA) [35] is adopted to approximate the electron exchange and correlation energy functional. To treat compositional disorder the KKR–ASA method is combined with the Coherent Potential Approximation (CPA) technique [41]. More details of the methodology can be found in Ref. [5].

5. Results and discussion

5.1. Lattice stabilities

In Table 1, structural properties and lattice stabilities calculated within both LDA and GGA approximations are compared with

Table 1
Lattice stabilities predicted from LDA and GGA first-principles electronic structure calculations, compared with values from the thermodynamic model developed in the present work and the U–Zr model [42].

Element	Phase	Space group	LDA (J/mol)	GGA (J/mol)	Model (J/mol)	U–Zr [42] (J/mol)
Np	Hcp	$P6_3/mmc$	74,860.61	49,106.39	70,000	–
U	Hcp	$P6_3/mmc$	–	–	–	50,000
Zr	Orthorhombic	Pnma	1613.97	5680.87	5837.36	38,000
Zr	Tetragonal	P4/nmm	1688.53	5630.14	4056.09	35,000

those obtained from our thermodynamic model and the U–Zr model [42]. These values are calculated by subtracting total energies of the pure elements in their reference states (orthorhombic in case of Np, and hcp in case of Zr), from the energies of both the elements in their corresponding unstable crystal structures (Np in hcp phase, and Zr in orthorhombic and tetragonal phases).

5.2. Phase diagram

The optimized parameters that are used to construct the Gibbs energy functions of the phases are listed in Table 2. In Fig. 1, the calculated phase diagram (Model 1) is compared with the provisional diagram published by Gibson et al. [8], along with DTA peaks obtained for various alloys from Ref. [7]. Fig. 2 compares the phase diagram (Model 1) with dilatometry and EPMA performed by Rodríguez et al. [11].

As noticeable from the phase diagrams, it is clear that there is a miscibility gap between the HT bcc phases of Np and Zr as confirmed in Refs. [6,7,10,8,9,14]. Even though the metallic radii and electronegativities of U, Pu, Np and Zr are similar, which might suggest mutual solubility, the contribution of 5f bonding electrons to the cohesive energies is greater in Np than U and Pu [7,8]. This leads to a larger disruption in 5f bonding when alloying with a non-5f element such as Zr and thus explains the non-ideal behavior of the Np–Zr system. The calculations are in agreement with most of the features predicted by Gibson et al. [8], minor discrepancies being in the positions of the liquidus, solidus, and bcc/hcp equilibrium lines. However, it must be pointed out that, at the final step of the optimization process, a stage was reached, where a compromise had to be made between these equilibrium lines and formation enthalpies of the bcc phase (see Section 5.3) so that the model satisfied various thermodynamic constraints applied to it. Additionally, DTA experiments [7] discussed in Section 2.1, showed that no well-defined peaks were observed above 913 K. It has been pointed out in Ref. [43] that it is highly probable that the melting points of (γ-Np, β-Zr) measured by Rodríguez et al.

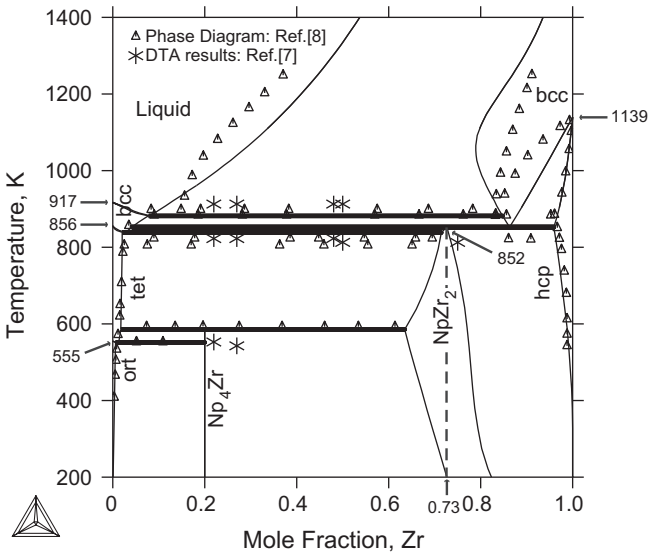

Fig. 1. Calculated phase diagram – Model 1 compared with phase diagram information from Ref. [8] and DTA results from Ref. [7].

[11], actually correspond to the liquid + β-Zr liquidus in the non-ideal phase diagram. This comparison is found to be consistent with our phase diagram and is shown in Fig. 2. Thus, the inconsistencies can be neglected given the limited number of experimental data points available, and also because it has been asserted several times [8,14] that the phase diagram published is only speculative. Table 3 shows the temperatures and compositions of the calculated and reported invariant reactions, which are in good agreement with each other.

Recently, a Np–Zr phase diagram, showing complete solid solubility of the bcc phase similar to the U–Zr and Pu–Zr systems, was calculated by Kurata [45]. This result was based on the assumption

Table 2
Model description and parameters for the phases in the Np–Zr system.

Phase	Model (Va = vacancy)	Evaluated parameters (J/mol)
Liquid	Random solution $(Np,Zr)_1$	${}^0L^{Liq}_{Np,Zr} = 126720.48 - 122.25 * T$
		${}^1L^{Liq}_{Np,Zr} = 27741.16 - 48.36 * T$
bcc	Sublattice model $(Np,Zr)_1(Va)_3$	${}^0L^{bcc}_{Np,Zr:Va} = 95381.69 - 84.08 * T$
		${}^1L^{bcc}_{Np,Zr:Va} = 83326.26 - 87.96 * T$
		${}^2L^{bcc}_{Np,Zr:Va} = -1133.70 - 12.25 * T$
hcp	Sublattice model $(Np,Zr)_1(Va)_{0.5}$	${}^0G^{hcp}_{Np:Va} - {}^0G^{ort}_{Np} = 70000$
		${}^0L^{hcp}_{Np,Zr:Va} = -48071.49 - 6.75 * T$
ortho	Random solution $(Np,Zr)_1$	${}^0G^{ort}_{Zr} - {}^0G^{hcp}_{Zr} = 5837.36 - 2.64 * T$
		${}^0L^{ort}_{Np,Zr} = -2528.41 + 35.95 * T$
tetra	Random solution $(Np,Zr)_1$	${}^0G^{tet}_{Zr} - {}^0G^{hcp}_{Zr} = 4056.09 + 1.36 * T$
		${}^0L^{tet}_{Np,Zr} = -3356.11 + 30.50 * T$
θ	Sublattice model $(Np)_4(Zr)_1$	${}^0G^{\theta}_{Np:Zr} - 4 * {}^0G^{ort}_{Np} - {}^0G^{hcp}_{Zr} = -2250.09 + 0.09 * T$
δ (Model 1)	Sublattice model $(Np,Zr)_2(Zr)_1$	${}^0G^{\delta}_{Np:Zr} - 2 * {}^0G^{ort}_{Np} - {}^0G^{hcp}_{Zr} = 2438.39 + 0.72 * T$
		${}^0G^{\delta}_{Zr:Zr} - 3 * {}^0G^{\omega}_{Zr} = 1800$
		${}^0L^{\delta}_{Np,Zr:Zr} = -9836.28 + 28.54 * T$
		${}^1L^{\delta}_{Np,Zr:Zr} = 3135 - 4.88 * T$
δ (Model2)	Sublattice model $(Np,Zr)_2(Zr)_1$	${}^0G^{\delta}_{Np:Zr} - 2{}^0G^{ort}_{Np} - {}^0G^{hcp}_{Zr} = 28330.92 - 28.07 * T$
		${}^0G^{\delta}_{Zr:Zr} - 3 * {}^0G^{\omega}_{Zr} = 0$
		${}^0L^{\delta}_{Np,Zr:Zr} = -69268.56 + 101.48 * T$
		${}^1L^{\delta}_{Np,Zr:Zr} = -44401.87 + 48.11 * T$

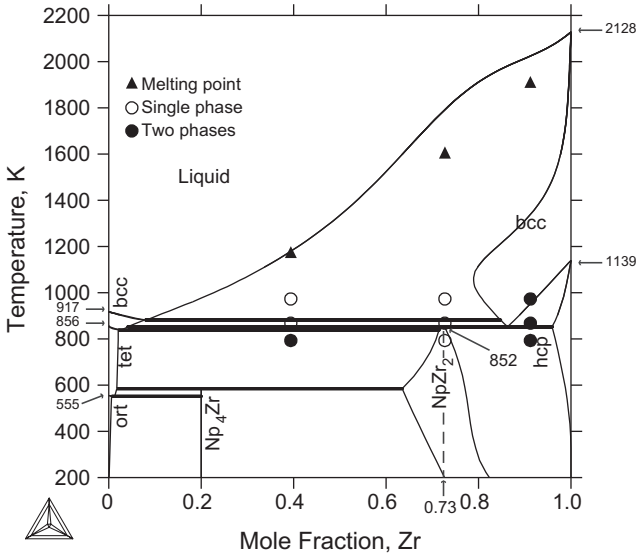

Fig. 2. Calculated phase diagram – Model 1 compared with data from Ref. [11].

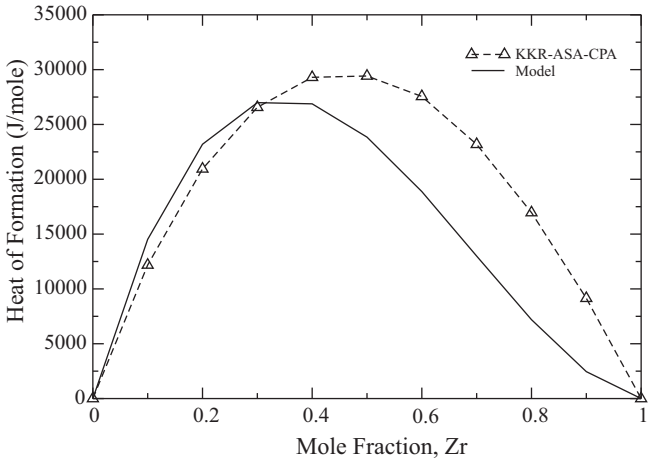

Fig. 3. Calculated formation enthalpy of bcc-based Np–Zr alloys as a function of composition, compared with results from KKR–ASA–CPA calculations under the GGA approach.

that interaction parameters of the bcc phase should almost be the same in both Np–Zr and Pu–Zr systems. However, due to reasons stated above, it is unlikely that the nature of chemical reaction in both the systems will be similar or that the bcc phase will from complete miscible solid solutions.

5.3. The bcc phase

To support the calculated phase diagram, formation enthalpies of the bcc phase obtained from this model are compared with results from calculations based on the KKR–ASA–CPA method in Fig. 3. High positive values indicate the tendency towards a miscibility gap in this phase, thus confirming our result.

Atomic volumes and bulk moduli of bcc-based Np–Zr alloys of various compositions, calculated using the KKR–ASA–CPA method, are plotted in Fig. 4. This plot also shows the linear variation between values obtained for pure bcc-Np and bcc-Zr, that would be expected based on Zen's Law [46]. Positive deviation in volumes and negative deviation in bulk moduli confirms the resistance in bonding between Np and Zr and thus, resulting in a miscibility gap in the bcc phase. The atomic volume of pure bcc-Np from these calculations is found to be 0.0185 nm^3, whereas the experimental value is 0.0218 nm^3 at 600 °C [47,48], and when extrapolated down to 20 °C, it is close to 0.0202 nm^3 [48]. It was expected that due to the more open structure of bcc, the atomic volume of γ-Np should be larger than that of α-Np (0.0192 nm^3 [48]). These inconsistencies can be explained by the reason that DFT does not take into account temperature

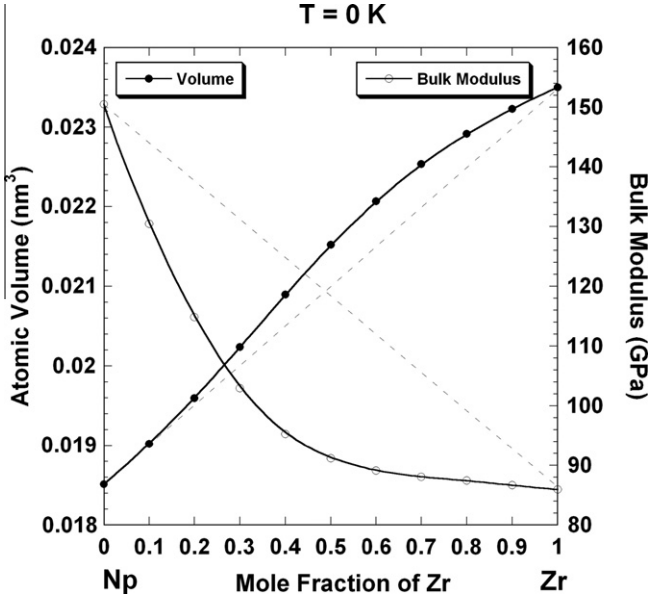

Fig. 4. Atomic volumes and bulk moduli of bcc phases of pure Np and pure Zr, and bcc-based Np–Zr alloys of various compositions calculated from the KKR–ASA–CPA method. Dotted lines denote the expected linear relationship based on Zen's Law [46].

effects, and therefore gives accurate results for the ground state phase, but less so for the high-temperature bcc phase, thus resulting in the observed discrepancy. Furthermore, the atomic volume

Table 3
Invariant reactions in the Np–Zr system.

Reaction	Okamoto [44]		Present work		Reaction type
	x(Zr)	Temp. (K)	x(Zr)	Temp. (K)	
$L \rightarrow \gamma$-Np + β-Zr	0.15	903	0.08	882	Eutectic
β-Zr $\rightarrow \gamma$-Np + α-Zr	0.83	883	0.86	852.3	Eutectoid
γ-Np + α-Zr $\rightarrow \delta$-$NpZr_2$ (Model 1)	0.70	823	0.73	852.2	Peritectoid
γ-Np + α-Zr $\rightarrow \delta$-$NpZr_2$ (Model 2)	0.70	823	0.79	843.5	Peritectoid
γ-Np $\rightarrow \beta$-Np + δ-$NpZr_2$	0.03	803	0.03	838.5	Eutectoid
β-Np + δ-$NpZr_2 \rightarrow \theta$-$Np_4Zr$	0.20	588	0.20	585.5	Peritectoid
β-Np $\rightarrow \alpha$-Np + θ-Np_4Zr	0.015	553	0.015	551	Eutectoid

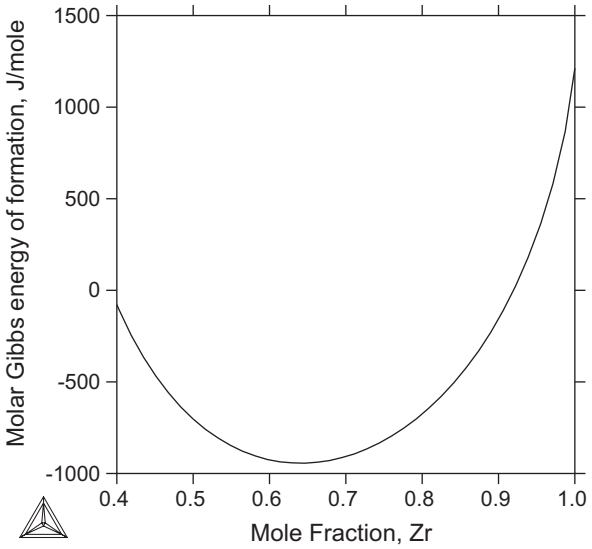

Fig. 5. Molar Gibbs energy of formation of the δ-phase at 840 K, calculated with the orthorhombic and hexagonal phases as reference states for Np and Zr, respectively.

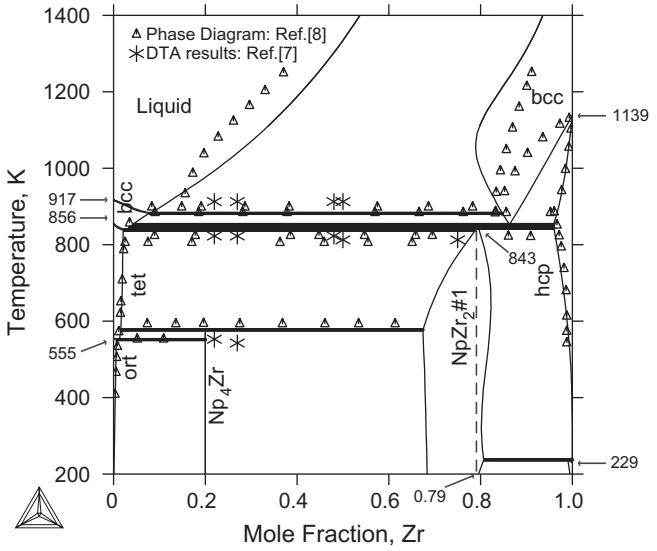

Fig. 7. Calculated phase diagram- Model 2 showing the miscibility gap in the δ-$NpZr_2$ phase, compared with phase diagram information from Ref. [8] and DTA results from Ref. [7].

of γ-Np calculated from KKR–ASA–CPA is consistent with the prior DFT result of 0.0175 nm^3 [49].

5.4. The δ-$NpZr_2$ phase

As mentioned in Section 2.4, the stability of the C32 structure in Zr increases when alloying with actinides, such as Uranium [5]. We predict a similar behavior in the Np–Zr system for the stability of the δ-phase. This phase is modeled as a sublattice phase with a random mixture of Np and Zr atoms occupying two sites in the first sublattice, namely the $\left(\frac{2}{3},\frac{1}{3},\frac{1}{2}\right)$ and $\left(\frac{1}{3},\frac{2}{3},\frac{1}{2}\right)$ positions, and pure Zr atoms occupying one site in the second sublattice, the $(0,0,0)$ position, thus resulting in a $(Np,Zr)_2$ $(Zr)_1$ configuration. This phase description is similar to the one proposed for the δ-UZr_2 phase, for which it was found from first-principles [5], that this configuration has the lowest energy out of all possible configurations. In accordance with the findings in Refs. [6,7,9], the decomposition of this phase into a mixture of γ-Np and α-Zr is assumed to take place at about 823 K. The only experimentally validated data on the composition range is mentioned in Ref. [11], where it has been found that this phase extends from 65.3 to 78.2 at.% Zr.

The molar Gibbs energy of formation of the δ-phase calculated from the model, is plotted versus composition at a temperature of 840 K in Fig. 5, with a maximum at about -1 KJ/mol. Formation enthalpy of the δ-phase in the U–Zr system, calculated from first-principles, is found to be -6.289 KJ/mol [5], and from calorimetry measurements, is -4.0 KJ/mol [50,51]; whereas, in the Pu–Zr system, the δ-phase never forms [16,17]. This decrease of stability, when going from U to Np and then to Pu, is expected and conforms with the calculations in Ref. [5], where it was shown that the critical d-band occupation change needed to form the δ-phase was reached for a lower concentration of U than Np when alloying with Zr, thus resulting in a relatively higher energy for formation in the Np–Zr system in comparison with the U–Zr system. Whereas, in the case of Pu, the d-band occupation change always remained lower than the critical value, thus explaining the absence of the δ-phase from the Pu–Zr phase diagram.

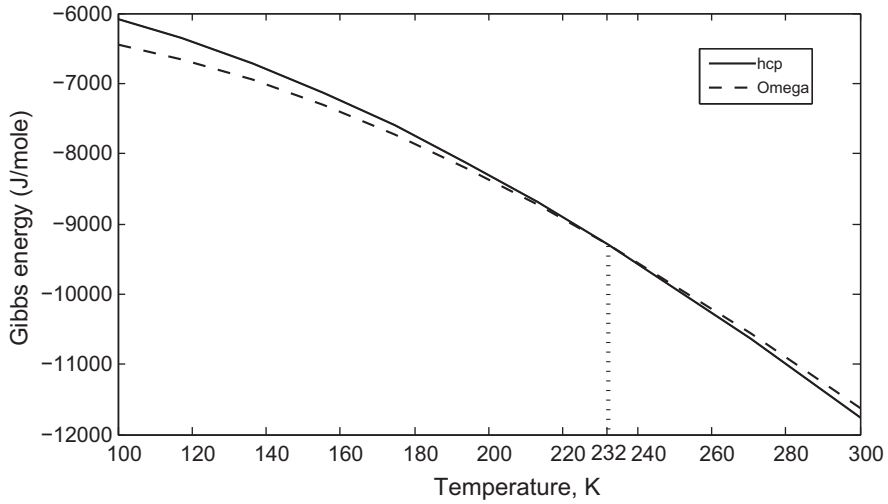

Fig. 6. Gibbs energy versus temperature plots for the hcp and ω-phases of pure Zr showing a cross-over at about 232 K.

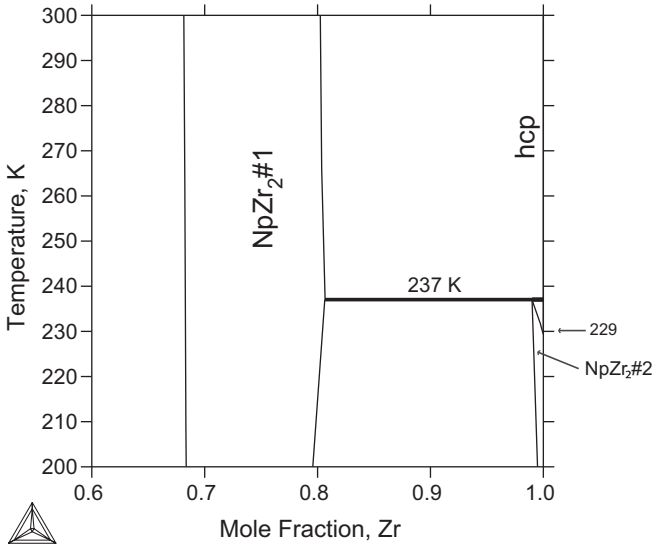

Fig. 8. Low temperature and Zr-rich section of the calculated phase diagram – Model 2 showing the stability of ω-phase ($NpZr_2$#2) over the hcp phase below 237 K and a miscibility gap between δ-$NpZr_2$#1 and $NpZr_2$#2.

To compare the stabilities/instabilities of the hcp and ω-phases of pure Zr from the SGTE database, the Gibbs energy functions (retrieved from this database) versus temperature curves for both the phases are plotted in Fig. 6. According to this plot, the energy curve of the ω-structure is lower than that of hcp up to about 230 K, beyond which it crosses over, indicating its instability above this temperature. However, according to the SGTE database, the Gibbs energy description of the ω-phase is defined only above 298 K, whereas that for the hcp phase is defined above 130 K. Thus, below 298 K, the energy curve for the ω-phase in Fig. 6 is obtained by mere extrapolation and the question of the more stable phase for Zr, remains unanswered.

Thus, in Model 1, a small value of $600 * 3$ J/mol (three for the total number of sites) was added to the Gibbs energy description of the ω-structure in the δ-phase (i.e. ${}^{0}G^{\delta}_{Zr:Zr} - 3{}^{*0}G^{\omega}_{Zr}$). And, in Model 2, this value was removed to make the ω-phase more stable. The phase diagram obtained in this case is shown in Fig. 7, and as expected, a miscibility gap is formed in the δ-phase. The second part of this phase forms nearly at $x(Zr) = 1$ and represents the ω-phase of pure Zr. Fig. 8 displays this phase diagram at low temperatures for the Zr-rich region.

6. Conclusions

A thermodynamic model of the Np–Zr system has been developed and is in good agreement with the postulated phase diagram by Gibson et al. [8], but not in complete agreement with results from dilatometry microanalysis data [11]. It is concluded that the Np–Zr system is non-ideal with a miscibility gap in the bcc phases of Np and Zr. The expected increase in melting point of the alloys does not occur in this system. Formation enthalpy of the bcc phase is found to be in close proximity to results obtained from KKR–ASA–CPA calculations. This confirms the validity of our model. First-principles calculations of lattice stabilities of various phases are used to verify values obtained from the thermodynamic model.

The δ-phase is modeled as a non-stoichiometric sublattice phase with a C32 structure, having random occupation of Np and Zr atoms on the $(\frac{2}{3},\frac{1}{3},\frac{1}{2})$ and $(\frac{1}{3},\frac{2}{3},\frac{1}{2})$ sites and Zr atoms occupying the (0,0,0) sites, similar to the δ-phase in the U–Zr system. Two possible models of this phase have been developed based on possibilities of the ground state phase of pure Zr, ω or hcp. However, since both electronic structure calculations and experimental studies (after extrapolation) point to the stability of ω-phase over the stability of hcp phase below 232 K, it is more likely that the ground state of Zr is the ω-phase and, that Model 2 in Fig. 7 represents the Np–Zr phase diagram.

To better guide future experimental studies on the Np–Zr alloy system, molar enthalpies of the system at temperatures within the range of 700–1000 K, are calculated and plotted for two alloy compositions in Fig. 9. Both these compositions are Zr-rich which would make the preparation of such samples relatively easier than to use more of neptunium, which poses limitations not only due to its radioactive nature, but also due to the difficulty in obtaining access to it for conducting experiments. As expected, a sudden

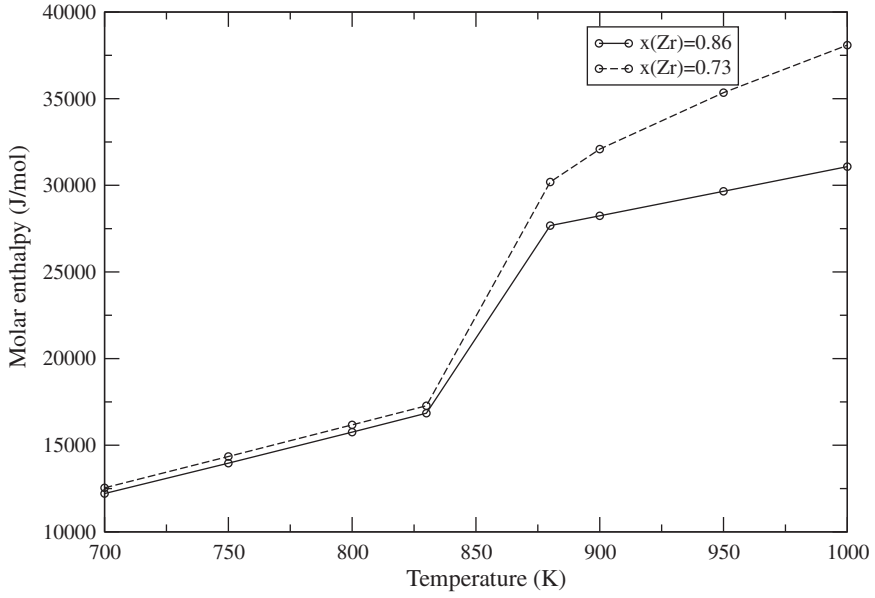

Fig. 9. Molar enthalpies of the system calculated at various temperatures for alloys of composition equal to $x(Zr) = 0.73$ – composition at the formation/decomposition of the δ-$NpZr_2$ phase, and at $x(Zr) = 0.86$, composition of the second invariant reaction in Table 3.

increase in enthalpy (~10–12 kJ/mol) is seen at around the phase transition temperatures (~850 °C) for both these alloys.

Acknowledgements

This work was supported by Lawrence Livermore National Laboratory under Task Order B575366 and Master Task Agreement B575363. The work of A.L., P.S. and P.T. has been performed under the auspices of the US DOE by the Lawrence Livermore National Laboratory under contract No. DE-AC52-07NA27344. The TAMU-CONACYT program is acknowledged for partial support of A.G. The authors would like to thank Tahir Cagin and Cem Sevik from the Department of Chemical Engineering, Texas A&M University for their valuable discussions on this work. First-principles calculations were performed in the Hydra cluster at the Texas A&M Supercomputing Facility, the Chemical Engineering Cluster at Texas A&M University as well as in the Ranger Cluster at the Texas Advanced Computing Center.

References

[1] E. Gerstner, Nature 460 (2009) 25–28.
[2] D.D. Keiser Jr., J.B. Kennedy, B.A. Hilton, S.L. Hayes, JOM 1 (2008) 29–32.
[3] A.J. Freeman, G.H. Lander (Eds.), Handbook on the Physics and Chemistry of the Actinides, vols. 1–5, North-Holland, Amsterdam and New York, 1984.
[4] A.J. Freeman, J.B. Darby (Eds.), The Actinides: Electronic Structure and Related Properties, vols. 1–2, Academic Press, 1974.
[5] A. Landa, P. Söderlind, P.E.A. Turchi, J. Alloys Compd. 478 (2009) 103–110.
[6] J.K. Gibson, R.G. Haire, Thermochim. Acta 207 (1992) 65–78.
[7] J.K. Gibson, R.G. Haire, J. Nucl. Mater. 201 (1993) 225–230.
[8] J.K. Gibson, R.G. Haire, M.M. Gensini, T. Ogawa, J. Alloys Compd. 213/214 (1994) 106–110.
[9] Y. Okamoto, R.G. Haire, J.K. Gibson, T. Ogawa, J. Alloys Compd. 232 (1996) 302–306.
[10] M.M. Gensini, R.G. Haire, J.K. Gibson, J. Alloys Compd. 213/214 (1994) 402–405.
[11] R.J. Rodríguez, C. Sari, A.J.C. Portal, J. Alloys Compd. 209 (1994) 263–268.
[12] E.R. Boyko, Acta Crystallogr. 10 (1957) 712–713.
[13] M. Akabori, T. Ogawa, A. Itoh, Y. Morii, J. Phys.: Condens. Matter 7 (1995) 8249–8257.
[14] T. Ogawa, J.K. Gibson, R.G. Haire, M.M. Gensini, M. Akabori, J. Nucl. Mater. 223 (1995) 67–71.
[15] N. Saunders, A.P. Miodownik, CALPHAD: Calculation of Phase Diagrams, in: Pergamon Materials Series, 1998.
[16] H. Okamoto, J. Phase Equilib. 14 (1993) 400–401.
[17] A.F. Berndt, J. Less-Common Met. 12 (1967) 82–83.
[18] S.K. Sikka, Y.K. Vohra, R. Chidambaran, Prog. Mater. Sci. 27 (1982) 245–310.
[19] H. Xia, A.L. Ruoff, Y.K. Vohra, Phys. Rev. B 44 (1991) 10374–10376.
[20] O. Botstein, A. Rabinkin, M. Talianker, Scripta Metall. 15 (1981) 151–155.
[21] F. Jona, P.M. Marcus, J. Phys.: Condens. Matter 15 (2003) 5009–5016.
[22] R. Ahuja, J.M. Wills, B. Johansson, O. Eriksson, Phys. Rev. B 48 (1993) 16269–16279.
[23] S.A. Ostanin, V.Y. Trubitsin, Phys. Stat. Sol. (b) 201 (1997) R9–R10.
[24] I. Schnell, R.C. Albers, J. Phys.: Condens. Matter. 18 (2006) 1483–1494.
[25] A.T. Dinsdale, CALPHAD 15 (1991) 317–425.
[26] O. Redlich, A.T. Kister, Ind. Eng. Chem. 40 (1948) 345–348.
[27] B. Sundman, B. Jansson, J.O. Andersson, CALPHAD 9 (1985) 153–190.
[28] G. Kresse, J. Hafner, Phys. Rev. B 47 (1993) 558–561.
[29] G. Kresse, J. Hafner, Phys. Rev. B 49 (1994) 14251–14269.
[30] G. Kresse, J. Furthmüller, Comput. Mater. Sci. 6 (1996) 15–50.
[31] G. Kresse, J. Furthmüller, Phys. Rev. B 54 (1996) 11169–11186.
[32] P.E. Blöchl, Phys. Rev. B 50 (1994) 17953–17979.
[33] G. Kresse, D. Joubert, Phys. Rev. B 59 (1999) 1758–1775.
[34] J.P. Perdew, A. Zunger, Phys. Rev. B 23 (1981) 5048–5079.
[35] J.P. Perdew, K. Burke, M. Ernzerhof, Phys. Rev. Lett. 78 (1997) 1396.
[36] H.J. Monkhorst, J.D. Pack, Phys. Rev. B 13 (1976) 5188–5192.
[37] O. Gunnarsson, O. Jepsen, O.K. Andersen, Phys. Rev. B 27 (1983) 7144–7168.
[38] I.A. Abrikosov, H.L. Skriver, Phys. Rev. B 47 (1993) 16532–16541.
[39] A.V. Ruban, H.L. Skriver, Comput. Mater. Sci. 15 (1999) 119–143.
[40] N.E. Christensen, S. Satpathy, Phys. Rev. Lett. 55 (1985) 600–603.
[41] J.S. Faulkner, Prog. Mater. Sci. 27 (1982) 1–187.
[42] P-Y Chevalier, E. Fischer, B. Cheynet, CALPHAD 28 (2004) 15–40.
[43] H. Okamoto, J. Phase Equilib. 17 (1996) 166–167.
[44] H. Okamoto, Phase Diagrams for Binary Alloys, Desk Handbook, 2000.
[45] M. Kurata, IOP Conf. Ser.: Mater. Sci. Eng. 9 (2010) 012023.
[46] E-an Zen, Am. Mineral., 41 (1956) 523–524.
[47] P.G. Mardon, J.H. Pearce, J.A.C. Marples, J. Less-Common Met. 3 (1961) 281–292.
[48] W.H. Zachariasen, Acta Cryst. 5 (1952) 664–665.
[49] P. Söderlind, B. Johansson, O. Eriksson, Phys. Rev. B 52 (1995) 1631–1639.
[50] K. Nagarajan, R. Babu, C.K. Mathews, J. Nucl. Mater. 203 (1993) 221–223.
[51] T. Ogawa, J. Nucl. Mater. 209 (1994) 107–108.